Estimation of the Velocity of a Walking Person in Indoor Environments from mmWave Signals

Rym Hicheri[1], Matthias Pätzold[1], and Néji Youssef[2]

[1]Faculty of Engineering and Science, University of Agder, NO-4898 Grimstad, Norway

[2]Université de Carthage, Ecole Supérieure des Communications de Tunis, 2083 El Ghazala, Tunisia

E-mail: [1]{rym.hicheri, matthias.paetzold}@uia.no, [2]neji.youssef@supcom.rnu.tn

***Abstract*—The present work is motivated by the growing interest in using millimeter-wave (mmWave) bands in future wireless indoor communications. For a variety of wireless indoor applications, such as remote medical care, healthcare services, and human-machine interaction, it is of crucial importance to estimate the velocity of walking persons in indoor environments with high precision. In this paper, we present a novel procedure for estimating the velocity of a walking person in indoor environments by using mmWave signals. The indoor environment is considered to be equipped with a distributed 2×2 multiple-input multiple-output (MIMO) system operating in the 60 GHz band. The proposed approach requires first to estimate the time-variant Doppler frequencies by fitting the spectrogram of the complex channel gain of a non-stationary indoor channel model to the spectrogram obtained from the received mmWave signals. The velocity of the moving person is then deduced from estimated time-varying Doppler frequencies. Numerical results, comparing the estimated Doppler frequencies and velocity with corresponding exact values, known from generated mmWave signals, are provided to demonstrate the validity of the proposed velocity estimation algorithm.**

I. Introduction

The study of human in-home activities recognition has received much attention during the last decades due to its wide scope of applications in, e.g., healthcare, security and surveillance, human-machine interaction, and robotics [1]−[3]. Within the context of healthcare, human activity recognition can enable various services, such as postoperative patients monitoring [2] and identifying unusual movements like falls and seizures [3]. Accurate estimation of health indication parameters is therefore essential for reliable health monitoring systems. Among these parameters, the walking speed, also referred to as gait velocity, has been shown to be an important health assessment metric [4]. A review of the literature shows that there are mainly three possible methods for the velocity estimation of walking persons in indoor environments. The first approach relies on the use of in-home camera-based systems. This technique detects the boundaries of a moving/fixed object, and iteratively updates these from frame to frame [5]. The second method is based on sensing technologies. In this case, the extraction of the walking speed can be achieved using a network of context-aware or wearable sensors [6]. In wearable sensor-based systems, instead, the sensors can be placed on clothes or even attached to human bodies [6]. Although, sensing technology is widely used in healthcare applications, the small size and the limited number of sensors that can be used on the human body, along with the battery life and the charging constitute its major limitations, especially for elderly healthcare services. To overcome these limitations, a third approach that is based on radio-frequency (RF) techniques can be employed. In this case, the desired health metrics can be obtained by utilizing the Doppler effect caused by walking persons. The so-called WiGait system, introduced in [7], is an example of an RF-based system developed for the purpose of extracting the gait velocity. Another notable related work can be found in [8], where Wi-Fi indoor localization with channel state information (CSI)-based speed estimation has been reported. In [9], the Emerald device has been proposed. This system has as purpose the three-dimensional motion tracking of persons based on the analysis of the phase of the complex channel gain. In [10], the so-called RF-Capture system for RF-based human activity tracking has been developed to capture the figure of a person when he/she is fully occluded. A common drawback of the works reported in [8] and [10] is that the accuracy of the developed methods is greatly affected by the rich multipath propagation characteristics of indoor channels.

With the growing market for the Internet of Things, the demand for fast wireless connections is growing rapidly. In this context, millimeter-wave (mmWave) communications have emerged as one of the most encouraging technologies for the next generation of wireless communications, thanks to their unlicensed available bandwidth as well as their high achievable data-rates [11]. Although, mmWave systems have been primarily proposed for outdoor communication, e.g., high-speed railway communication [12], several studies have been dedicated to the evaluation of the usability and feasibility of mmWaves in indoor areas, e.g., [13]–[17]. With the development of the IEEE Wi-Fi standard 802.11ad which uses the

978-1-5386-4920-6/18/$31.00 ©2018 IEEE

unlicensed 60 GHz spectrum, the Wireless Gigabit Alliance (WiGig) 1.0 specification was released in 2011 [15]. WiGig enabled devices allow robust high-speed indoor wireless communications with a throughput of up to 7 Gbps and a working range of 10 m. With the commercialization of the 60 GHz Wi-Fi technology, mmWaves have been drawing increasing attention. For example, in the context of future indoor healthcare services, the mmVital system was introduced in [16] to monitor the breathing and heart rate of persons in indoor environments by transmitting 60 GHz mmWave signals and analyzing the received signal strength. The interest in mmWave indoor channels is also motivated by the fact that mmWave signals are extremely sensitive to blockage between the transmitter (T_x) and the receiver (R_x) due to fixed/moving objects/persons. To address this topic, numerous mmWave channel models have been presented in the literature. An overview of existing mmWave channel models has been reported in [17], where measurement- and map-based models have been shown to emulate the behavior of mmWave indoor channels. Although emphasis has been laid on indoor-to-indoor communications, no generic channel model has been developed. Here, we profit from the fact that mmWaves can be modeled using optical wave propagation, and employ the two-dimensional non-stationary indoor channel model introduced in [18], to describe the indoor propagation phenomena by taking into account the influence of walking persons.

Motivated by the limitations of the techniques reported in [5]−[10] and the importance of mmWave bands for future applications, our main objective is to contribute to the topic of human activity detection by proposing a new method to estimate the velocity of a single moving person in an indoor environment using mmWave bands while taking into account the effects of both moving and fixed scatterers. The proposed procedure is inspired by the iterative non-linear least square approximation (INLSA) algorithm which was originally introduced in [19] and has later been refined in in [20] to design measurement-based wideband channel simulators. Although, the INLSA algorithm has been applied to both the time-frequency correlation function [20] and time-variant impulse response [21], its applicability is so far limited to wide-sense stationary channels. Here, we extend the method further to the velocity estimation of moving persons in non-stationary indoor environments. For simplicity, the walking person is represented by a single moving scatterer, which represents the person's center of gravity. On the other hand, the fixed scatterers represent the walls, the furniture, and the decoration items (frames, books, etc.). The room is assumed to be equipped with a distributed 2×2 multiple-input multiple-output (MIMO) system. In the first part of this work, the gains, phases, and time-variant Doppler frequencies are optimized by fitting the spectrogram of the model in [18] to that of the received signals. Then, the time-variant speed and angle-of-motion (AOM) of the moving person as well as the time-variant angles-of-departure (AODs) and time-variant angles-of-arrival (AOAs) are deduced from the estimated Doppler frequencies. The determination of the channel parameters is based on the minimization of the Euclidean norm of the fitting errors. Exact closed-form expressions have been derived for the estimated path gains corresponding to the moving scatterer (moving person) as well as the fixed scatterers. The accuracy of the proposed procedure has been verified by comparing the obtained estimated parameters of interest, i.e., time-variant Doppler frequencies, time-variant speed and AOM, with those of known mmWave test signals generated by computer simulations.

This paper is organized as follows. Section II presents some useful background material. The proposed estimation procedure is described in Section III. Numerical examples are provided in Section IV. Finally, Section V concludes the paper.

II. Background Material

A. Problem Description

Interest in velocity estimation-based monitoring devices has increased significantly in recent decades. However, the performance of RF-based systems is strongly affected by the rich scattering structure of indoor environments. The main objective of this paper is to present a novel estimator of the velocity of a moving person in an indoor environment by utilizing the effects of the person's motion on the Doppler characteristics of the propagation medium in the presence of both moving and fixed scatterers. Fig. 1 presents a typical room architecture with four distributed antennas (two transmit antennas A_1^T and A_2^R and two receive antennas A_1^R and A_2^R) and the single moving person. Our objective is to estimate the time-variant velocity of the moving person. For simplicity, we consider a two-dimensional indoor multipath propagation scenario as illustrated in Fig. 2, which consists of a room with length A and width B centered at the origin O. The room is equipped with a distributed 2×2 MIMO system, i.e., the T_x (R_x) is equipped with two omni-directional antennas A_1^T and A_2^T (A_1^R and A_2^R) which are located at the positions (x_1^T, y_1^T) and (x_2^T, y_2^T) ((x_1^R, y_1^R) and (x_2^R, y_2^R)), respectively. It is also assumed that there is only one person moving in the room. For simplicity, this person is modeled by a single moving scatterer S^M, located at the initial position (x^M, y^M), whose trajectory is described by a

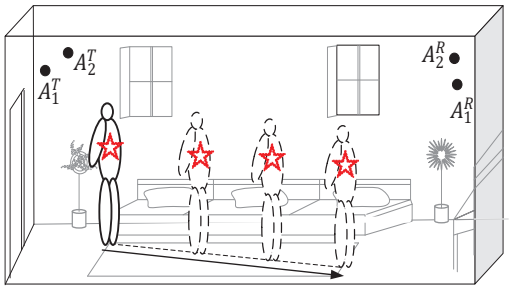

Fig. 1. Typical room architecture with the distributed antennas, the fixed scatterers and the moving scatterer (the walking person).

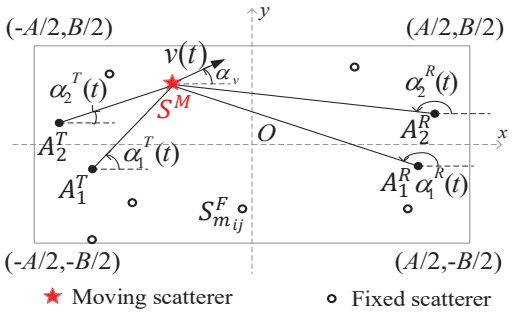

Fig. 2. Description of the multipath propagation scenario in the 2×2 MIMO indoor channel.

time-variant speed $v(t)$ and a constant AOM α_v. The time-variant positions $x(t)$ and $y(t)$ along the x- and y-axis of the moving scatterer S^M can be obtained according to [18, Eqs. (4) and (5)]. The scenario includes also walls and objects which are modeled by M_{ij} fixed scatterers $S^F_{m_{ij}}$ $(m = 1, 2, \ldots, M_{ij})$. Furthermore, single-bounce scattering is assumed.

B. Spectrogram

Considering the previously introduced propagation scenario and assuming perfect CSI at the receiver side, the complex channel gain $\mu_{ij}(t)$ between the ith receive antenna and jth transmit antenna $(i, j = 1, 2)$ is given by [18]

$$\mu_{ij}(t) = c_{ij} \exp\left[j\theta_{ij}(t)\right] + \sum_{m_{ij}=0}^{M_{ij}} c_{m_{ij}} \exp\left(j\theta_{m_{ij}}\right) \quad (1)$$

where the first term refers to the component resulting from the moving scatterer and the second term represents the multipath components coming from the $M_{ij}+1$ fixed scatterers. Since both the T_x and the R_x are fixed, the line-of-sight (LOS) component does not experience any Doppler shift and thus, can be modeled as a fixed scatterer with a gain c_0 and a phase θ_0. In (1), the quantity c_{ij} $(c_{m_{ij}})$ refers to the gain of the moving (m_{ij}th fixed) scatterer. The time-variant channel phase $\theta_{ij}(t)$ is expressed in terms of the time-variant Doppler frequency $f_{ij}(t)$ as $\theta_{ij}(t) = 2\pi \int_0^t f_{ij}(x)dx + \theta_{ij,0}$ [18], where $\theta_{ij,0}$ is the initial channel phase and

$$f_{ij}(t) = -f_{\max}(t)\left[\cos\left(\alpha_j^T(t) - \alpha_v\right) + \cos\left(\alpha_i^R(t) - \alpha_v\right)\right] \quad (2)$$

in which $f_{\max}(t) = f_0 v(t)/c_0$ denotes the time-variant maximum Doppler frequency, with f_0 and c_0 being the carrier frequency and the speed of light, respectively. In (2), $\alpha_j^T(t)$ and $\alpha_i^R(t)$ stand for the AOD and AOA and are expressed according to [18, Eq. (6) and (7)]. In (1), the phases $\theta_{m_{ij}}$ are assumed to be independent and identically distributed random variables and are uniformly distributed over the interval $(0, 2\pi]$. For simplicity, in the following, the sum term $\sum_{m_{ij}=0}^{M_{ij}} c_{m_{ij}} \exp\left(j\theta_{m_{ij}}\right)$ in (1) will be replaced by a single complex random variable term $C_{F_{ij}} \exp(j\vartheta_{F_{ij}})$, where $C_{F_{ij}} = \sqrt{\left(\sum_{m_{ij}=0}^{M_{ij}} c_{m_{ij}} \cos(\theta_{m_{ij}})\right)^2 + \left(\sum_{m_{ij}=0}^{M_{ij}} c_{m_{ij}} \sin(\theta_{m_{ij}})\right)^2}$ and $\vartheta_{F_{ij}} = \text{atan2}(\sum_{m_{ij}=0}^{M_{ij}} c_{m_{ij}} \sin(\theta_m m_{ij}), \sum_{m_{ij}=0}^{M_{ij}} c_{m_{ij}} \cos(\theta_{m_{ij}}))$, in which atan2 refers to the multi-valued inverse tangent function. According to [18], for time intervals in which the Doppler frequency $f_{ij}(t)$ can be assumed to vary linearly with time, i.e., can be approximated by a first-order Taylor series expansion, the spectrogram $S_{ij}(f,t)$ of the complex channel gain $\mu_{ij}(t)$ in (1) is expressed as

$$S_{ij}(f,t) = S_{ij}^{(a)}(f,t) + S_{ij}^{(c)}(f,t) \quad (3)$$

where the auto-term $S_{ij}^{(a)}(f,t)$ is given by

$$S_{ij}^{(a)}(f,t) = c_{ij}^2 G\left(f, f_{ij}(t), \sigma_{ij,1}^2\right) + G\left(f, 0, \frac{\sigma_0^2}{2}\right) C_{F_{ij}}^2 \quad (4)$$

in which $G(a,b,c) = \exp[-(a-b)^2/(2c)]/(\sqrt{2\pi c})$, $\sigma_0^2 = 1/(2\pi\sigma_w)^2$, and $\sigma_{ij,1}^2 = (\sigma_0^2 + \sigma_w^2 k_{ij}^2)/2$, with $k_{ij} = d\left(f_{ij}(t)\right)/dt|_{t=0}$ and σ_w^2 being the spread of the Gaussian window used for the derivation of the spectrogram. The expression of the cross-term $S_{ij}^{(c)}(f,t)$ is given by [18, Eq. (35)]

$$S_{ij}^{(c)}(f,t) = \frac{2c_{ij}C_{F_{ij}}}{\sigma_w\sqrt{\pi}} \Re\left\{G\left(f, f_{ij}(t), \sigma_{ij,2}^2\right) \cdot G^*\left(f, 0, \sigma_0^2\right) \exp\left(j\left(\theta_{ij}(t) - \vartheta_{F_{ij}}\right)\right)\right\} \quad (5)$$

where $\sigma_{ij,2}^2 = \sigma_0^2 - jk_{ij}/(2\pi)$. It should be mentioned that the Doppler frequencies generally do not vary linearly with time and cannot be approximated by a first-order Taylor series expansion. The expression of the spectrogram in (3) remains only valid for time durations T_0 if the spread σ_w^2 of the Gaussian window is smaller than T_0 during which the approximation in [18, Eq. (16)] is accurate. This can be achieved by dividing the observation time into subintervals during which the Doppler frequencies can be approximated by linear functions, whose parameter k_{ij} is updated from one subinterval to the following. In this case, for the total observation time, the parameter k_{ij} is time-variant and will be denoted by $k_{ij}(t)$.

III. Estimation of the Velocity

This section deals with estimating the velocity of a moving person in an indoor environment. First, we will estimate the time-variant Doppler frequencies.

A. Estimation of the Time-Variant Doppler Frequency

In practice, the spectrogram $\hat{S}_{ij}(f_q, t_p)$ of the complex channel gain is computed from samples of the measured received signal with discrete frequencies $f_q = q\Delta f \in [-B/2, B/2]$, $q = 1, .., Q$ and time instances $t_p = p\Delta t \in [0, T]$, $p = 1, .., P$, where B is the frequency bandwidth and T denotes the observation time interval. The quantities Δf and Δt refer to the frequency and time sampling periods, respectively. Here, the problem at hand is to determine a set of parameters $\mathcal{P}_1(t_p) = \{\tilde{c}_{ij}, \tilde{k}_{ij,p}, \tilde{f}_{ij,p}, \tilde{C}_{F_{ij}}, \tilde{\vartheta}_{F_{ij}}\}$ in such a way that the spectrogram $\tilde{S}_{ij}(f_q, t_p)$ of

the channel model in [18] matches $\hat{S}_{ij}(f_q,t_p)$. For this purpose, we introduce the objective function for determining $\mathcal{P}_1(t_p)$ as

$$E_1(\mathcal{P}_1(t_p))=\left|\left|\hat{S}_{ij}(f_q,t_p)-\tilde{S}_{ij}(f_q,t_p)\right|\right|_2^2. \quad (6)$$

The objective function in (6) is equivalent to

$$\begin{aligned}E_1(\mathcal{P}_1(t_p))=&\left|\left|\hat{S}_{ij}(f_q,t_p)-\tilde{c}_{ij}^2 G\Big(f_q,\tilde{f}_{ij,p},\tilde{\sigma}_{ij,1,p}^2\Big)\right.\right.\\ &-G\Big(f_q,0,\frac{\sigma_0^2}{2}\Big)\tilde{C}_{F_{ij}}^2-\frac{2\tilde{c}_{ij}\tilde{C}_{F_{ij}}}{\sigma_w\sqrt{\pi}}\Re\Big\{G\Big(f,\tilde{f}_{ij,p},\tilde{\sigma}_{ij,2,p}^2\Big)\\ &\left.\left.\cdot G^*\left(f,0,\sigma_0^2\right)\exp\Big(j\left(\tilde{\theta}_{ij,p}-\tilde{\vartheta}_{F_{ij}}\right)\Big)\Big\}\right|\right|_2^2 \quad (7)\end{aligned}$$

where the quantities $\tilde{c}_{ij}$, $\tilde{f}_{ij,p}$, $\tilde{C}_{F_{ij}}$, and $\tilde{\vartheta}_{F_{ij}}$ refer to the estimated values of c_{ij}, $f_{ij,p}=f_{ij}(t_p)$, $C_{F_{ij}}$, and $\vartheta_{F_{ij}}$, and $\tilde{\theta}_{ij,p}=2\pi\int_0^{t_p}\tilde{f}_{ij}(x_p)\,dx_p+\theta_{ij,0}$. Here, $\tilde{\sigma}_{ij,1,p}^2=(\sigma_0^2+\sigma_w^2\tilde{k}_{ij,p}^2)/2$ and $\tilde{\sigma}_{ij,2,p}^2=\sigma_0^2-j\tilde{k}_{ij,p}/(2\pi)$, in which $\tilde{k}_{ij,p}$ is the estimated value of $k_{ij,p}=k_{ij}(t_p)$. For arbitrary chosen initial values of $\tilde{c}_{ij}^{(0)}$, $\tilde{k}_{ij,p}^{(0)}$, $\tilde{f}_{ij,p}^{(0)}$, $\tilde{C}_{F_{ij}}^{(0)}$, and $\tilde{\vartheta}_{F_{ij}}^{(0)}$, the new estimates of $\tilde{c}_{ij}^{(l+1)}$, $\tilde{k}_{ij,p}^{(l+1)}$, $\tilde{f}_{ij,p}^{(l+1)}$, $\tilde{C}_{F_{ij}}^{(l+1)}$, and $\tilde{\vartheta}_{F_{ij}}^{(l+1)}$ at every iteration l ($l=0,1,...$) are obtained as in (8) [see the top of the next page], where $\hat{\mathbf{s}}_{ij}$ is a column vector containing the stacked values of $\hat{S}_{ij}(f_q,t_p)$ for increasing values of q. For fixed values of $\tilde{k}_{ij,p}^{(l)}$, $\tilde{f}_{ij,p}^{(l)}$, $\tilde{C}_{F_{ij}}^{(l)}$, and $\tilde{\vartheta}_{F_{ij}}^{(l)}$, it can be shown that (8) is minimized if $x=\tilde{c}_{ij}^{(l+1)}$ satisfies

$$\begin{aligned}&2x^3\left|\left|\mathbf{y}_{ij}^{(l)}\right|\right|_2^2+3x^2\left(\mathbf{y}_{ij}^{(l)}\right)^T\mathbf{f}_{ij}^{(l)}+x\Big[\left|\left|\mathbf{f}_{ij}^{(l)}\right|\right|_2^2\\ &-2\left(\hat{\mathbf{s}}_{ij}^{(l)}-\mathbf{g}^{(l)}\right)^T\mathbf{y}_{ij}^{(l)}\Big]-\left(\mathbf{f}_{ij}^{(l)}\right)^T\left(\hat{\mathbf{s}}_{ij}^{(l)}-\mathbf{g}^{(l)}\right)=0 \quad (9)\end{aligned}$$

where $(\cdot)^T$ is the transpose operator. The symbols $\mathbf{g}^{(l)}$, $\mathbf{f}_{ij}^{(l)}$, and $\mathbf{y}_{ij}^{(l)}$ are column vectors containing the stacked values of the functions$(\tilde{C}_{F_{ij}}^{(l)})^2G(f_q,0,\sigma_0^2/2)$, $2\tilde{C}_{F_{ij}}^{(l)}/(\sigma_w\sqrt{\pi})\Re\{G(f_q,\tilde{f}_{ij,p}^{(l)},(\tilde{\sigma}_{ij,2,p}^{(l)})^2)G^*(f_q,0,\sigma_0^2)\exp(j(\theta_{ij,p}^{(l)}-\tilde{\vartheta}_{F_{ij}}^{(l)}))\}$, and $G(f_q,\tilde{f}_{ij,p}^{(l)},(\tilde{\sigma}_{ij,1,p}^{(l)})^2)$ for increasing values of q, respectively. Since the equation in (9) has real-valued coefficients, at least one of its roots is real. The number of real and complex roots of (9) are determined by the sign of the corresponding discriminant Δ_0 which is expressed in (10) [see the top of the next page]. If $\Delta_0\geq 0$ ($\Delta_0<0$), the cubic equation in (9) has three real roots (one real root and two complex conjugate roots). In all cases, the roots x_k, $k=1,2,3$, are expressed as $x_k=-(b_0+\zeta^kA_0+B_0/(\zeta^kA_0))/(3a_0)$, where $\zeta=0.5(j\sqrt{3}-1)$ is a cube root of unity, $a_0=2||\mathbf{y}_{ij}^{(l)}||_2^2$, $b_0=3(\mathbf{y}_{ij}^{(l)})^T\mathbf{f}_{ij}^{(l)}$, $B_0=b_0^2-3a_0[(||\mathbf{f}_{ij}^{(l)}||^2-2(\hat{\mathbf{s}}_{ij}-\mathbf{g}^{(l)})^T\mathbf{y}_{ij}^{(l)}]$, and $A_0=[(C_0\pm\sqrt{-27\Delta_0a_0^2})/2]^{1/3}$, in which $C_0=2b_0^2-9a_0b_0[(||\mathbf{f}_{ij}^{(l)}||^2-2(\hat{\mathbf{s}}_{ij}-\mathbf{g}^{(l)})^T\mathbf{y}_{ij}^{(l)}]-27a_0^2(\mathbf{f}_{ij}^{(l)})^T(\hat{\mathbf{s}}_{ij}^{(l)}-\mathbf{g}^{(l)})$. The new estimate of the path gain $\tilde{c}_{ij}^{(l+1)}$ corresponds to the real-valued root x_k that minimizes the right-hand side of (8). By inserting the new estimate $\tilde{c}_{ij}^{(l+1)}$ in (8), the optimization problem in (8) reduces to the one in (11) [see the top of the next page]. Then, it can be shown that (11) is minimized if the new estimate $x=\tilde{C}_{F_{ij}}^{(l+1)}$ satisfies the following equation

$$\begin{aligned}&3x^2\mathbf{u}^T\mathbf{k}_{ij}^{(l)}+x\left[\left|\left|\mathbf{k}_{ij}^{(l)}\right|\right|^2-2\left(\hat{\mathbf{s}}_{ij}-\left(\tilde{c}_{ij}^{(l+1)}\right)^2\mathbf{y}_{ij}^{(l)}\right)^T\mathbf{u}\right]\\ &+2x^3||\mathbf{u}||^2-\left(\mathbf{k}_{ij}^{(l)}\right)^T\left(\hat{\mathbf{s}}_{ij}-\left(\tilde{c}_{ij}^{(l+1)}\right)^2\mathbf{y}_{ij}^{(l)}\right)=0 \quad (12)\end{aligned}$$

where $\mathbf{u}$ and $\mathbf{k}_{ij}^{(l)}$ are column vectors containing the stacked values of the functions $G(f_q,0,\sigma_0^2/2)$ and $2\Re\{G(f,f_{ij,p}^{(l)},(\sigma_{ij,2,p}^{(l)})^2)G^*(f,0,\sigma_0^2)\exp(j(\theta_{ij,p}^{(l)}-\vartheta_{F_{ij}}^{(l)}))\}\tilde{c}_{ij}^{(l+1)}/(\sigma_w\sqrt{\pi})$ for increasing values of q, respectively. The number of real roots of (12) are determined by the sign of its discriminant Δ_1 expressed in (13) [see the top of the next page]. Regardless of the sign of Δ_1, the roots x_k, $k=1,2,3$, of (12) are expressed according to $x_k=-(b_1+\zeta^kA_1+B_1/(\zeta^kA_1))/(3a_1)$, where $a_1=2||\mathbf{u}||_2^2$, $b_1=3\mathbf{u}^T\mathbf{k}_{ij}^{(l)}$, $B_1=b_1^2-3a_1[||\mathbf{k}_{ij}^{(l)}||_2^2-2(\hat{\mathbf{s}}_{ij}-(\tilde{c}_{ij}^{(l+1)})^2\mathbf{y}_{ij}^{(l)})^T\mathbf{u}]$, and $A_1=[(C_1\pm\sqrt{-27\Delta_1a_1^2})/2]^{1/3}$, in which $C_1=2b_1^3-9a_1b_1[||\mathbf{k}_{ij}^{(l)}||_2^2-2(\hat{\mathbf{s}}_{ij}-(\tilde{c}_{ij}^{(l+1)})^2\mathbf{y}_{ij}^{(l)})^T\mathbf{u}]-27a_1^2(\mathbf{k}_{ij}^{(l)})^T(\hat{\mathbf{s}}_{ij}-(\tilde{c}_{ij}^{(l+1)})^2\mathbf{y}_{ij}^{(l)})$. The new estimate $\tilde{C}_{F_{ij}}^{(l+1)}$ is the non-negative real-valued root x_k of (12) that minimizes the right-hand side of (8). By substituting $\tilde{C}_{F_{ij}}^{(l+1)}$ in (8), the problem in (8) reduces to the three-dimensional optimization problem in (14) [see the top of the next page]. Then, the new estimates of $\tilde{k}_{ij,p}^{(l+1)}$, $\tilde{f}_{ij,p}^{(l+1)}$, and $\tilde{\vartheta}_{F_{ij}}^{(l+1)}$ are numerically determined by minimizing the right-hand side of (14). The iterative procedure in (8)−(14) proceeds as long as the relative change in the objective function $E_1\left(\mathcal{P}_1(t_p)\right)$ is greater than a predefined error ε_1, and must be carried out at each time instant t_p.

B. Estimation of the Time-Variant Velocity

In this section, the time-variant velocity $\vec{v}(t_p)$, i.e., speed $v(t_p)$ and AOM α_v, of the moving person are deduced from the estimated Doppler frequencies $\tilde{f}_{ij,p}$ ($i,j=1,2$). At this point, it should be stressed that it is important that the transmit and receive antennas are located far enough from each other to ensure different time-variant AODs $\alpha_j^T(t_p)$ and AOAs $\alpha_i^R(t_p)$ ($i,j=1,2$). In the following, the estimated values of $v_p=v(t_p)$, α_v, $\alpha_{j,p}^T=\alpha_j^T(t_p)$, and $\alpha_{i,p}^R=\alpha_i^R(t_p)$ will be denoted by $\tilde{v}_p$, $\tilde{\alpha}_v$, $\tilde{\alpha}_{j,p}^T$, and $\tilde{\alpha}_{i,p}^R$, respectively. Here, the problem is to determine a set of parameters $\mathcal{P}_2(t_p)=\left\{\tilde{v}_p,\tilde{\alpha}_v,\tilde{\alpha}_{j,p}^T,\tilde{\alpha}_{i,p}^R\right\}$ in such a way that the estimated Doppler frequencies $\tilde{f}_{ij,p}$ are as close as possible to those of the channel model. To do so, we

$$\left(\tilde{c}_{ij}^{(l+1)},\tilde{k}_{ij,p}^{(l+1)},\tilde{f}_{ij,p}^{(l+1)},\tilde{C}_{F_{ij}}^{(l+1)},\tilde{\vartheta}_{F_{ij}}^{(l+1)}\right)=\underset{\mathcal{P}_1(t_p)}{\arg\min}\left|\left|\hat{\mathbf{s}}_{ij}-\tilde{c}_{ij}^2 G\Big(f_q,\tilde{f}_{ij,p},\tilde{\sigma}_{ij,1,p}^2\Big)-G\left(f_q,0,\frac{\sigma_0^2}{2}\right)\tilde{C}_{F_{ij}}^2\right.\right.$$
$$\left.\left.-\frac{2\tilde{c}_{ij}\tilde{C}_{F_{ij}}}{\sigma_w\sqrt{\pi}}\Re\Big\{G\Big(f,\tilde{f}_{ij,p},\tilde{\sigma}_{ij,2,p}^2\Big)\,G^*\left(f,0,\sigma_0^2\right)\exp\left(j\left(\tilde{\theta}_{ij,p}-\tilde{\vartheta}_{F_{ij}}\right)\right)\Big\}\right|\right|_2^2 \quad (8)$$

$$\Delta_0=108\left\|\mathbf{y}_{ij}^{(l)}\right\|_2^2\left[2\Big(\hat{\mathbf{s}}_{ij}-\mathbf{g}^{(l)}\Big)^T\mathbf{y}_{ij}^{(l)}-\left\|\mathbf{f}_{ij}^{(l)}\right\|_2^2\right]\left\|\mathbf{f}_{ij}^{(l)}\right\|_2^2\Big(\mathbf{y}_{ij}^{(l)}\Big)^T\Big(\hat{\mathbf{s}}_{ij}-\mathbf{g}^{(l)}\Big)+108\left(\Big(\mathbf{y}_{ij}^{(l)}\Big)^T\mathbf{f}_{ij}^{(l)}\right)^3\Big(\mathbf{f}_{ij}^{(l)}\Big)^T\Big(\hat{\mathbf{s}}_{ij}^{(l)}-\mathbf{g}^{(l)}\Big)$$
$$+9\left(\Big(\mathbf{y}_{ij}^{(l)}\Big)^T\mathbf{f}_{ij}^{(l)}\left[\left\|\mathbf{f}_{ij}^{(l)}\right\|_2^2-2\Big(\hat{\mathbf{s}}_{ij}^{(l)}-\mathbf{g}^{(l)}\Big)^T\mathbf{y}_{ij}^{(l)}\right]\right)^2-8\left\|\mathbf{y}_{ij}^{(l)}\right\|_2^2\left[\left\|\mathbf{f}_{ij}^{(l)}\right\|_2^2-2\Big(\hat{\mathbf{s}}_{ij}^{(l)}-\mathbf{g}^{(l)}\Big)^T\mathbf{y}_{ij}^{(l)}\right]^3-108\left\|\mathbf{y}_{ij}^{(l)}\right\|_2^4\left(\Big(\mathbf{f}_{ij}^{(l)}\Big)^T\Big(\hat{\mathbf{s}}_{ij}^{(l)}-\mathbf{g}^{(l)}\Big)\right)^2. \quad (10)$$

$$\left(\tilde{k}_{ij,p}^{(l+1)},\tilde{f}_{ij,p}^{(l+1)},\tilde{C}_{F_{ij}}^{(l+1)},\tilde{\vartheta}_{F_{ij}}^{(l+1)}\right)=\underset{\tilde{k}_{ij,p},\tilde{f}_{ij,p},\tilde{C}_{F_{ij}},\tilde{\vartheta}_{F_{ij}}}{\arg\min}\left|\left|\hat{\mathbf{s}}_{ij}-\left(\tilde{c}_{ij}^{(l+1)}\right)^2 G\Big(f_q,\tilde{f}_{ij,p},\tilde{\sigma}_{ij,1,p}^2\Big)-G\left(f_q,0,\frac{\sigma_0^2}{2}\right)\tilde{C}_{F_{ij}}^2\right.\right.$$
$$\left.\left.-\frac{2\tilde{c}_{ij}^{(l+1)}\tilde{C}_{F_{ij}}}{\sigma_w\sqrt{\pi}}\Re\Big\{G\Big(f,\tilde{f}_{ij,p},\tilde{\sigma}_{ij,2,p}^2\Big)\,G^*\left(f,0,\sigma_0^2\right)\exp\left(j\left(\tilde{\theta}_{ij,p}-\tilde{\vartheta}_{F_{ij}}\right)\right)\Big\}\right|\right|_2^2. \quad (11)$$

$$\Delta_1=-108\left|\left|\mathbf{u}\right|\right|_2^2\mathbf{u}^T\mathbf{k}_{ij}^{(l)}\left[\left|\left|\mathbf{k}_{ij}^{(l)}\right|\right|^2-2\left(\hat{\mathbf{s}}_{ij}-\left(\tilde{c}_{ij}^{(l+1)}\right)^2\mathbf{y}_{ij}^{(l)}\right)^T\mathbf{u}\right]\left(\mathbf{k}_{ij}^{(l)}\right)^T\left(\hat{\mathbf{s}}_{ij}-\left(\tilde{c}_{ij}^{(l+1)}\right)^2\mathbf{y}_{ij}^{(l)}\right)$$
$$+108\left(\mathbf{u}^T\mathbf{k}_{ij}^{(l)}\right)^3\left(\mathbf{k}_{ij}^{(l)}\right)^T\left(\hat{\mathbf{s}}_{ij}-\left(\tilde{c}_{ij}^{(l+1)}\right)^2\mathbf{y}_{ij}^{(l)}\right)+9\left(\mathbf{u}^T\mathbf{k}_{ij}^{(l)}\left[\left|\left|\mathbf{k}_{ij}^{(l)}\right|\right|^2-2\left(\hat{\mathbf{s}}_{ij}-\left(\tilde{c}_{ij}^{(l+1)}\right)^2\mathbf{y}_{ij}^{(l)}\right)^T\mathbf{u}\right]\right)^2$$
$$-8\left|\left|\mathbf{u}\right|\right|_2^2\left[\left|\left|\mathbf{k}_{ij}^{(l)}\right|\right|^2-2\left(\hat{\mathbf{s}}_{ij}-\left(\tilde{c}_{ij}^{(l+1)}\right)^2\mathbf{y}_{ij}^{(l)}\right)^T\mathbf{u}\right]^3-108\left|\left|\mathbf{u}\right|\right|_2^4\left(\left(\mathbf{k}_{ij}^{(l)}\right)^T\left(\hat{\mathbf{s}}_{ij}-\left(\tilde{c}_{ij}^{(l+1)}\right)^2\mathbf{y}_{ij}^{(l)}\right)\right)^2. \quad (13)$$

$$\left(\tilde{k}_{ij,p}^{(l+1)},\tilde{f}_{ij,p}^{(l+1)},\tilde{\vartheta}_{F_{ij}}^{(l+1)}\right)=\underset{\tilde{k}_{ij,p},\tilde{f}_{ij,p},\tilde{\vartheta}_{F_{ij}}}{\arg\min}\left|\left|\hat{\mathbf{s}}_{ij}-\left(\tilde{c}_{ij}^{(l+1)}\right)^2 G\Big(f_q,\tilde{f}_{ij,p},\tilde{\sigma}_{ij,1,p}^2\Big)-\left(\tilde{C}_{F_{ij}}^{(l+1)}\right)^2 G\big(f_q,0,\sigma_0^2\big)\right.\right.$$
$$\left.\left.-\frac{2\tilde{c}_{ij}^{(l+1)}\tilde{C}_{F_{ij}}^{(l+1)}}{\sigma_w\sqrt{\pi}}\Re\left\{G\left(f_q,\tilde{f}_{ij,p},\tilde{\sigma}_{ij,2,p}^2\right)G^*\left(f_q,0,\sigma_0^2\right)\exp\left(j\left(\tilde{\theta}_{ij,p}-\tilde{\vartheta}_{F_{ij}}\right)\right)\right\}\right|\right|_2^2. \quad (14)$$

introduce the objective function $E_2\left(\mathcal{P}_2(t_p)\right)$ as

$$E_2(\mathcal{P}_2(t_p))=\left\|\begin{matrix}\tilde{f}_{11,p}-\tilde{f}\left(\tilde{v}_p,\tilde{\alpha}_{1,p}^T,\tilde{\alpha}_{1,p}^R,\tilde{\alpha}_v\right)\\ \tilde{f}_{12,p}-\tilde{f}\left(\tilde{v}_p,\tilde{\alpha}_{2,p}^T,\tilde{\alpha}_{1,p}^R,\tilde{\alpha}_v\right)\\ \tilde{f}_{21,p}-\tilde{f}\left(\tilde{v}_p,\tilde{\alpha}_{1,p}^T,\tilde{\alpha}_{2,p}^R,\tilde{\alpha}_v\right)\\ \tilde{f}_{11,p}-\tilde{f}\left(\tilde{v}_p,\tilde{\alpha}_{2,p}^T,\tilde{\alpha}_{2,p}^R,\tilde{\alpha}_v\right)\end{matrix}\right\|_2^2 \quad (15)$$

where $\tilde{f}(a,b,c,d)=-f_0 a[\cos(b-d)+\cos(c-d)]/c_0$. For the arbitrarily chosen initial values of $\tilde{v}_p^{(0)}$, $\tilde{\alpha}_v^{(0)}$, $(\tilde{\alpha}_{i,p}^R)^{(0)}$ and $(\tilde{\alpha}_{j,p}^T)^{(0)}$, the new estimates of the speed $\tilde{v}_p^{(l+1)}$, AOM $\tilde{\alpha}_v^{(l+1)}$, AOD $(\tilde{\alpha}_{j,p}^T)^{(l+1)}$ $(i=1,2)$, and AOA $(\tilde{\alpha}_{j,p}^R)^{(l+1)}$ $(j=1,2)$ are obtained according to

$$\left(\tilde{v}_p^{(l+1)},\tilde{\alpha}_v^{(l+1)},\left(\tilde{\alpha}_{j,p}^T\right)^{(l+1)},\left(\tilde{\alpha}_{i,p}^R\right)^{(l+1)}\right)=$$
$$\underset{\mathcal{P}_2(t_p)}{\arg\min}\left\|\begin{matrix}\tilde{f}_{11,p}-\tilde{f}\left(\tilde{v}_p,\tilde{\alpha}_{1,p}^T,\tilde{\alpha}_{1,p}^R,\tilde{\alpha}_v\right)\\ \tilde{f}_{12,p}-\tilde{f}\left(\tilde{v}_p,\tilde{\alpha}_{2,p}^T,\tilde{\alpha}_{1,p}^R,\tilde{\alpha}_v\right)\\ \tilde{f}_{21,p}-\tilde{f}\left(\tilde{v}_p,\tilde{\alpha}_{1,p}^T,\tilde{\alpha}_{2,p}^R,\tilde{\alpha}_v\right)\\ \tilde{f}_{22,p}-\tilde{f}\left(\tilde{v}_p,\tilde{\alpha}_{2,p}^T,\tilde{\alpha}_{2,p}^R,\tilde{\alpha}_v\right)\end{matrix}\right\|_2^2. \quad (16)$$

The iterative procedure in (15) and (16) proceeds as long as the objective function $E_2\left(\mathcal{P}_2(t_p)\right)$ is higher than the predefined error level ε_2, and must be performed at each time instant t_p.

IV. Numerical Results

In this section, we present some numerical results for the validation of the algorithm described in Section III. To this end, we compare the exact time-variant Doppler frequencies and speed with the corresponding estimated quantities. It should be mentioned that this task cannot be achieved using measurements data, for which the exact person's velocity, i.e., speed and AOM, is unknown. Therefore, to have access to the exact velocity, and equivalently the Doppler frequencies, a priori, we consider the simulation model in [18] to generate a waveform sample of the complex channel gains $\hat{\mu}_{ij}(t_p)$ and compute the corresponding spectrogram. This simulated spectrogram will play the role of $\hat{S}(f_q,t_p)$.

For the performance analysis, we considered three different scenarios to model the speed $v(t)$ of the single moving person and an observation time interval of $[0,5\text{s}]$. In Scenario I, the person is moving with constant speed $v_1(t)=1.1$ m/s. In Scenario II, the person

starts walking with a constant speed, decelerates at the time instant $t = 2.5\,\text{s}$, until he/she stops at $t = 4.5\,\text{s}$. In this case, the speed $v_2(t)$ is given by

$$v_2(t) = \begin{cases} 1 & \text{if } 0 \leq t \leq 2.5\,\text{s} \\ -0.25t + 1.125 & \text{if } 2.5 \leq t \leq 4.5\,\text{s} \\ 0 & \text{if } 4.5 \leq t \leq 5\,\text{s} \end{cases}. \quad (17)$$

Finally, in Scenario III, the speed is modeled using a sinusoidal function and is given by $v_3(t) = 0.3\sin(\pi t/3 + 0.5) + 0.35$. The choice of the speed values of the different scenarios has been made in accordance with [22]. The length A and width B of the room have been chosen to be 14 m and 7 m, respectively. The locations of the transmit and receive antennas A_1^T, A_2^T, A_1^R, and A_2^R were $(-4.9, 1)$, $(-4.9, -1)$, $(4.5, 2)$, and $(4.5, -2)$, respectively. The moving person is initially located at the position $(1, 2)$ and walks toward the termination point of coordinate (5,0). He/she is assumed to be walking along a linear trajectory. In all scenarios, the AOM has been based on the initial location of S^M and the termination point. The number of fixed scatterers is set to 8 ($M_{ij} = 7$) with $\sum_{m_{ij}=0}^{M_{ij}} c_{m_{ij}}^2 = 1$. Also, the carrier frequency f_0 has been set to 60 GHz. The parameter σ_w^2 has been chosen to be $\sigma_w^2 = 1/\sqrt{2\pi|k_{ij}|}$. For simplicity, the initial phase of the channel $\theta_{ij,0}$ has been set to 0. In the following, the error levels ε_1 and ε_2 are 0.001.

Figs. 3(a), (b), and (c) present the time-variant Doppler frequencies $f_{ij}(t)$ $(i, j = 1, 2)$ for Scenario I, Scenario II, and Scenario III, respectively. As can be observed, there is a good match between the exact Doppler frequencies and those obtained by applying the proposed algorithm. In Fig. 4, we present a comparison between the exact speed $v(t)$ of the moving person and that obtained by numerical estimation. As can be seen, there is a good fit between both quantities for the three considered scenarios.

Comparison with other methods: To the best of the authors' knowledge, the only method that has been developed in the context of human activity monitoring and can be considered for comparison purposes is that reported in [7]. Unfortunately, no details regarding the employed algorithm are available in the literature. Additionally, several mobile station's velocity estimation techniques have been developed in the context of mobile radio communications, e.g., level-crossing rate (LCR)- and covariance-based estimators. A review of these methods [23], [24] shows that they require a priori knowledge of the expressions of the higher-order statistics, such as the LCR, the covariance properties, and the rate of maxima, of the fading channel. Although these statistics have been extensively investigated in the literature for numerous fading channel models, their study has been limited to wide-sense stationary channels. Since there exist, to date, no results regarding the statistics of non-stationary channels, existing mobile station's velocity estimators cannot be applied either. Therefore, comparison results with other velocity estimators cannot be presented. However, the good match between the exact and estimated parameters of interest observed in Figs. 3 and 4 confirms the validity of the proposed estimation procedure and its applicability to various speed models.

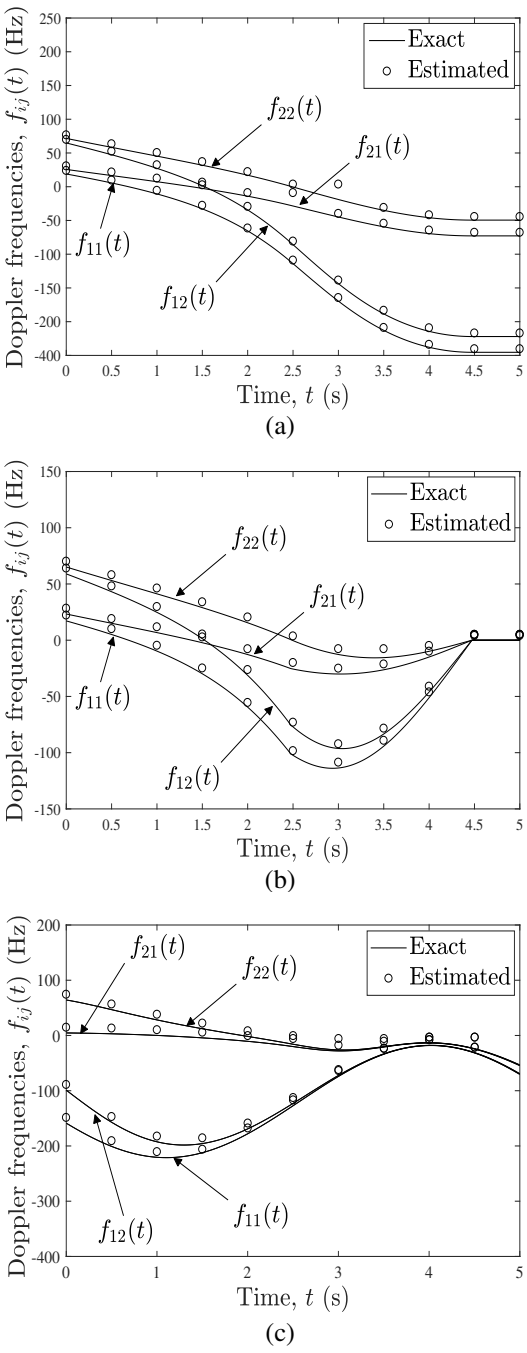

Fig. 3. Time-variant Doppler frequencies $f_{ij}(t)$ $(i, j = 1, 2)$ for (a) Scenario I, (b) Scenario II, and (c) Scenario III.

V. Conclusion

In this paper, we have proposed a new iterative procedure to accurately estimate the velocity of a single moving person in indoor environments equipped with a distributed 2×2 MIMO system using mmWave signals. The proposed estimation procedure is divided

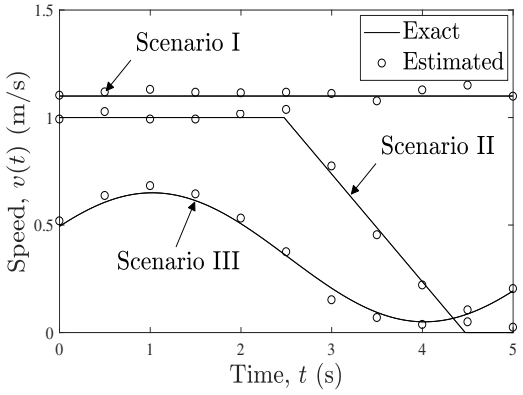

Fig. 4. Time-variant speed $v(t)$ of the moving scatterer S^M.

into two parts. First, the time-variant Doppler frequencies are estimated by fitting the spectrogram of the channel model to the spectrogram computed from the received mmWave signals. Then, the algorithm estimates the time-variant velocity, i.e., speed and AOM, of the moving person by means of the estimated Doppler frequencies. The good match between the exact Doppler frequencies and speed of the moving person and the corresponding estimated quantities for different speed models confirms the validity of the proposed estimation method. Although, this algorithm has been developed in the context of indoor mmWave channels, its applicability can be extended to the general case of non-stationary indoor channels.

ACKNOWLEDGEMENT

This work was supported by the WiCare Project funded by the Research Council of Norway under grant number 261895/F20.

REFERENCES

[1] M. Ermes, J. Pärkkä, J. Mäntyjärvi, and I. Korhonen, "Detection of daily activities and sports with wearable sensors in controlled and uncontrolled conditions," *IEEE Trans. Inf. Technol. in Biomedicine*, vol. 12, no. 1, pp. 20–26, Jan. 2008.

[2] C. Strohrmann, H. Harms, C. Kappeler-Setz, and G. Troster, "Monitoring kinematic changes with fatigue in running using body-worn sensors," *IEEE Trans. Inf. Technol. in Biomedicine*, vol. 16, no. 5, pp. 983–990, Sept. 2012.

[3] B. Mariani, M. Castro Jiménez, F. J. G. Vingerhoets, and K. Aminian, "On-shoe wearable sensors for Gait and turning assessment of patients with Parkinson's disease," *IEEE Trans. Biomedical Eng.*, vol. 60, no. 1, pp. 155–158, Jan. 2013.

[4] A. Middleton, S. L. Fritz, and M. Lusardi, "Walking speed: the functional vital sign," *Journal of Aging and Physical Activity*, vol. 23, no. 2, pp. 314–322, May 2015.

[5] H. Sakaino, "Video-based tracking, learning, and recognition method for multiple moving objects," *IEEE Trans. Circuits and Systems for Video Technol.*, vol. 23, no. 10, pp. 1661–1674, 2013.

[6] S. C. Mukhopadhyay, "Wearable sensors for human activity monitoring: A review," *IEEE Sensors J.*, vol. 15, no. 3, pp. 1321–1330, Mar. 2015.

[7] C.-Y. Hsu, Y. Liu, Z. Kabelac, R. Hristov, D. Katabi, and C. Liu, "Extracting Gait velocity and stride length from surrounding radio signals," in *Proceedings of the ACM Conf. on Human Factors in Computing Systems (CHI'17)*, Denver, USA, May 2017, pp. 2116–2126.

[8] Z.-P. Jiang and al., "Communicating is crowdsourcing: Wi-Fi indoor localization with CSI-based speed estimation," *J. of Computer Science and Technol.*, vol. 29, no. 4, pp. 589–604, Jul. 2014.

[9] "Emerald (2015) [Online]," Available: http://www.emerald-forhome.com/.

[10] F. Adib and al., "Capturing the coarse human figure through a wall," *ACM Trans. Graphics*, vol. 34, Issue 6, no. 219, pp. 1–13, Nov. 2015.

[11] European Telecommunications Standards Institute, "Millimetre Wave Transmission (mWT); Applications and Use Cases of Millimetre Wave Transmission [Online]," Tech. Rep. ETSI GS mWT 002 v1.1.1, Aug. 2015, Available: http://www.etsi.org.

[12] M. Gao and al., "Dynamic mmWave beam tracking for high speed railway communications," in *IEEE Wireless Commun. and Net. Conf. Workshops (WCNCW'18)*, 2018, pp. 278–283.

[13] K. Dong, X. Liao, and S. Zhu, "Link blockage analysis for indoor 60 Ghz radio systems," *Electronics Letters*, vol. 48, no. 23, pp. 1506–1508, Nov. 2012.

[14] F. Firyaguna, J. Kibilda, C. Galiotto, and N. Marchetti, "Coverage and spectral efficiency of indoor mmWave networks with ceiling-mounted access points," in *IEEE Global Commun. Conf. (GLOBECOM'17)*, Dec. 2017.

[15] "Intel Gigabit Wireless (2011) [Online]," Available: http://www.intel.com/content/dam/www/public/us/en/documents/product-briefs/tri-band-wireless-ac17265-brief.pdf.

[16] Z. Yang, P. H. Pathak, Y. Zeng, X. Liran, and P. Mohapatra, "Monitoring vital signs using millimeter wave," in *17th ACM Int. Symp. on Mobile Ad Hoc Networking and Computing (ACM'16)*, 2016, pp. 211–220.

[17] Y.-G. Lim, Y. J. Cho, Y. Kim, and C.-B. Chae, "Map-based millimeter-wave channel models: An overview, guidelines, and data," *arXiv preprint arXiv:1711.09052*, 2017.

[18] A. Abdelgawwad and M. Pätzold, "On the influence of walking people on the Doppler spectral characteristics of indoor channels," in *28th IEEE Int. Symp. on Pers., Indoor, and Mobile Radio Commun. (PIMRC'17), Montreal, QC, Canada*, Oct. 2017.

[19] D. Umansky and M. Pätzold, "Design of measurement-based wideband mobile radio channel simulators," in *4th Int. Symp. on Wireless Commun. Systems (ISWCS'07)*, Trondheim, Norway, Oct. 2007, pp. 229–235.

[20] A. Fayziyev and M. Pätzold, "An improved iterative nonlinear least square approximation method for the design of measurement-based wideband mobile radio channel simulators," in *Int. Conf. on Advanced Technol. for Commun. (ATC'11), Da Nang, Vietnam*, 2011, pp. 106–111.

[21] A. Fayziyev, M. Pätzold, E. Masson, Y. Cocheril, and M. Berbineau, "A measurement-based channel model for vehicular communications in tunnels," in *Wireless Communications and Networking Conference (WCNC'14), IEEE*, 2014, pp. 116–121.

[22] J. E. Graham, S. R. Fisher, I.-M. Bergés, Y.-F. Kuo, and G. V. Ostir, "Walking speed threshold for classifying walking independence in hospitalized older adults," *Physical Therapy*, vol. 90, no. 11, pp. 1591–1597, Nov. 2010.

[23] G. Azemi, E. Holmbakken, V. Karawalevu, and B. Senadji, "The importance of accurate velocity estimation in designing handover algorithms for microcellular systems," *Queensland University of Technology Press*, 2002.

[24] H. Zhang and A. Abdi, "Non-parametric mobile speed estimation in fading channels: Performance analysis and experimental results," *IEEE Trans. Wireless Commun.*, vol. 8, no. 4, Apr. 2009.